Electronic Supplementary Information: Field-driven reversible networks from colloidal rods

José Fojo,[a,b] Rodolfo Subert,[c] Laura Rodríguez-Arco, [b,d] Modesto T. López-López,[b,d] Marjolein Dijkstra,*[c] Carla Fernández-Rico,*[e] and Laura Alvarez*[a]

[a]CNRS, Univ. Bordeaux, CRPP, UMR5031, 33600 Pessac, France.
[b]Universidad de Granada, Departamento de Física Aplicada, Campus de Fuentenueva, E-18071 Granada, Spain
[c] Soft Condensed Matter & Biophysics, Debye Institute for Nanomaterials Science, Utrecht University, The Netherlands
[d]Instituto de Investigación Biosanitaria Ibs.GRANADA E-18014 Granada, Spain
[e]Department of Materials, ETH Zürich, 8093 Zurich, Switzerland
*To whom correspondence should be addressed;
E-mail: laura.alvarez-frances@u-bordeaux.fr

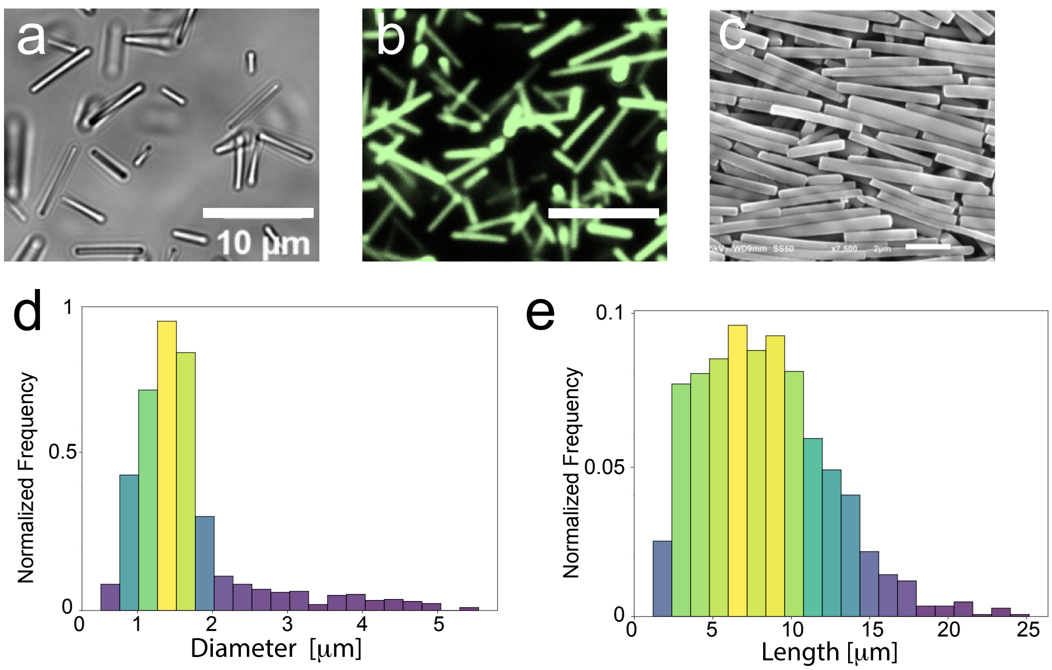

Figure S1: **SU8-rod characterization** (a,b) Optical microscopy images of the SU8-rods in (a) Bright field and (b) fluorescence modes. (c) SEM images of the SU8-rods. (d,e) Histograms of the SU8-rods for the diameter and length in μm

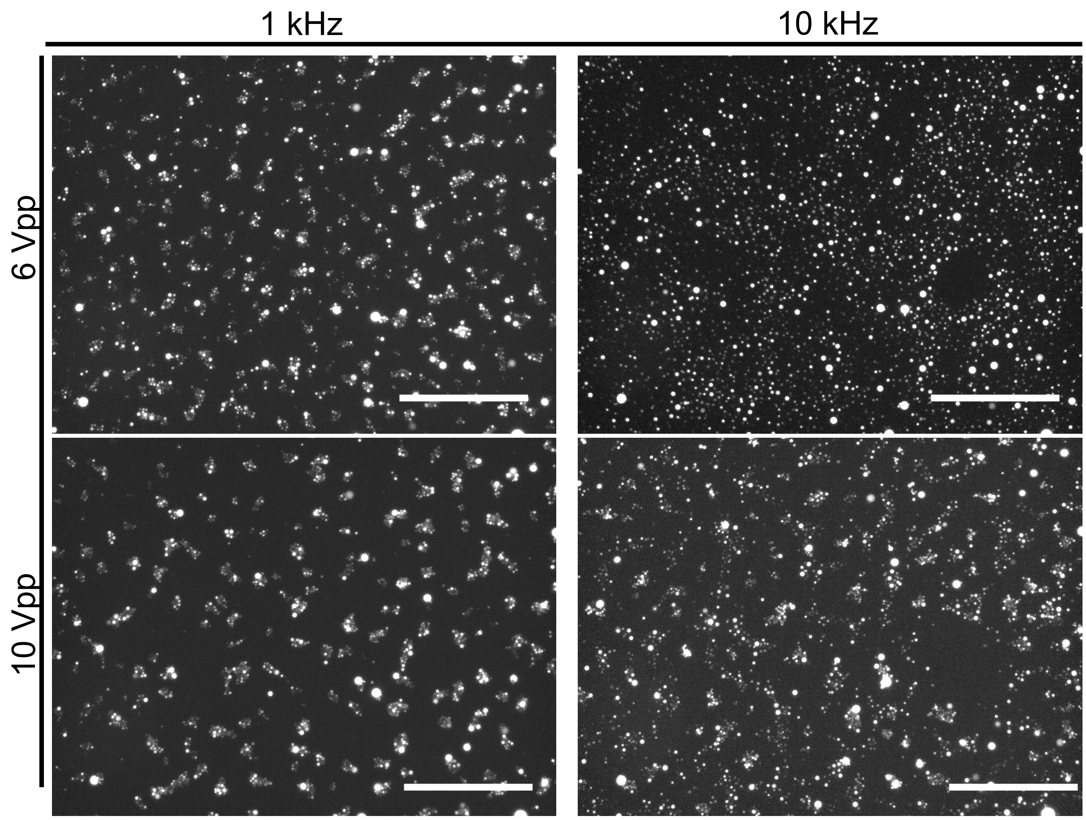

Figure S2: **Control experiments with SU8 spheres** Fluorescence images of SU8-spheres with area fraction $\phi_c \approx 0.38$ under different AC electric field conditions, forming isolated cluster at the same conditions where the rods form an interconnected network. The scale bars depict 50μm.

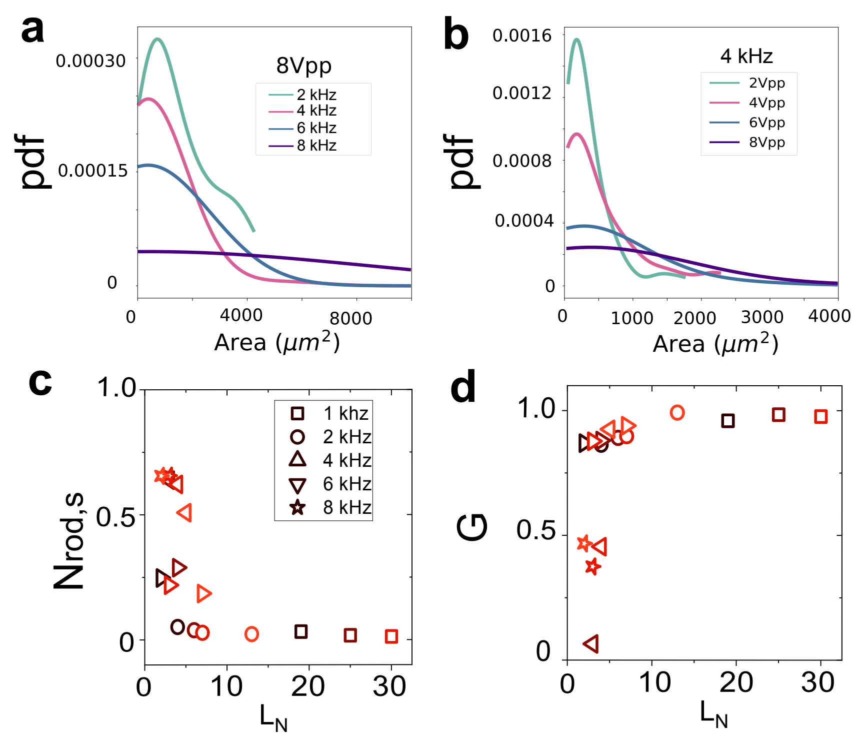

Figure S3: **Characterization of planar network** Probability density function of pore areas of the SU8-rod network structure for (a) 8 Vpp at different frequencies and (b) 4 kHz at increasing voltages. Dependence on the network thickness L_N of (c) number of standing rods $N_{rod,s}$ and (d) connectivity G. The color coding in (c) and (d) indicated th increasing voltage from dark red to light red.

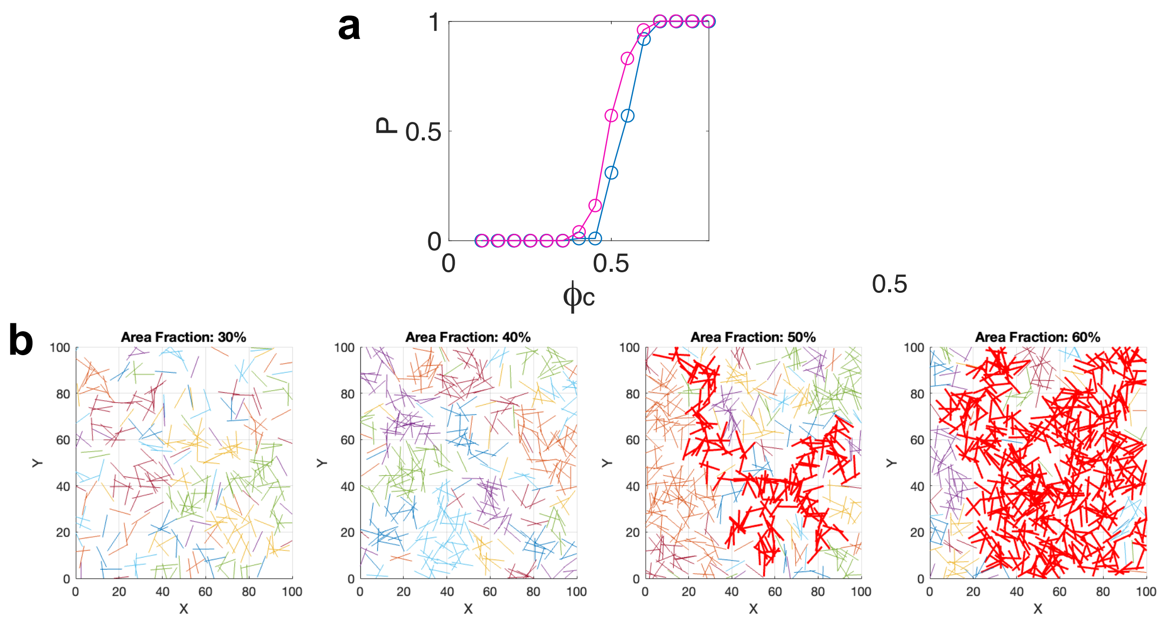

Figure S4: **Numerical estimation for increasing area fractions of non-interacting and planar rods**. (a) Probability of cluster formation as a function of area fractions ϕ_c for homogenous (blue) and polydisperse of $\approx$ 30% (magenta) systems. (b) Corresponding images of randomly distributed and oriented rods for a homogenous systems of planar rods. Each cluster is depicted in a different colour. Red colour depicts a fully connected cluster on the field of view.

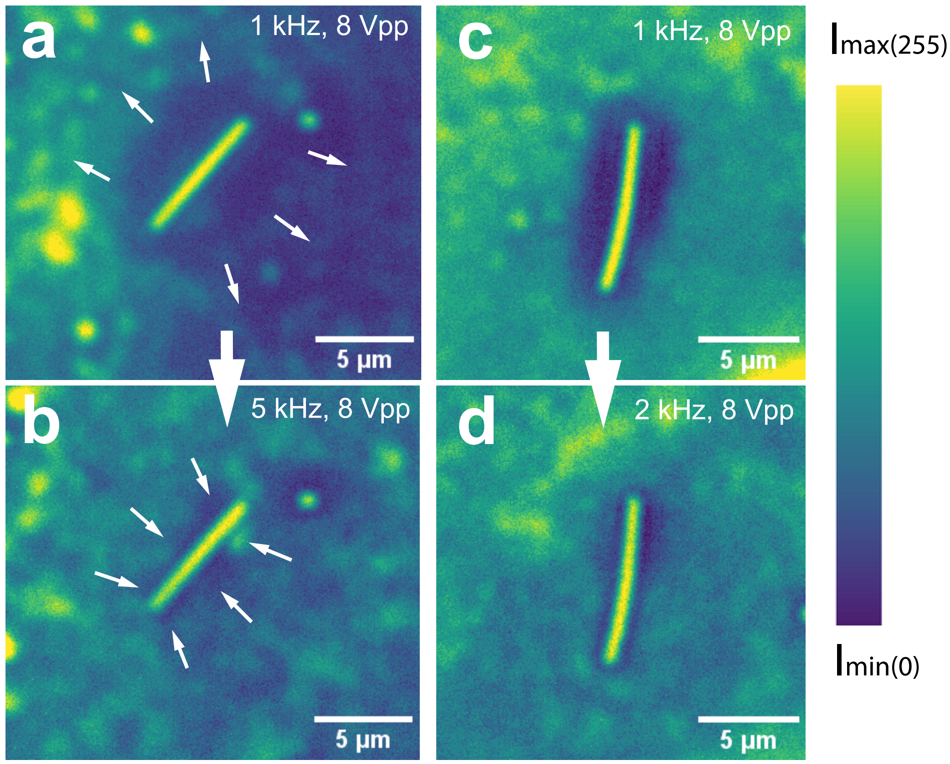

Figure S5: **Characterization of EHD flows around the rods** Integrated intensities of tracers measured over 60 s at 1 kHz (a,b) and 5 kHz (b) and 2 kHz (d). The color coding represents the intensity levels in an 8-bit format from I_{min} (dark green - 0) to I_{max} (bright green - 255). The white arrows indicate the direction of the tracers away (a) or towaeds (b) the rod.

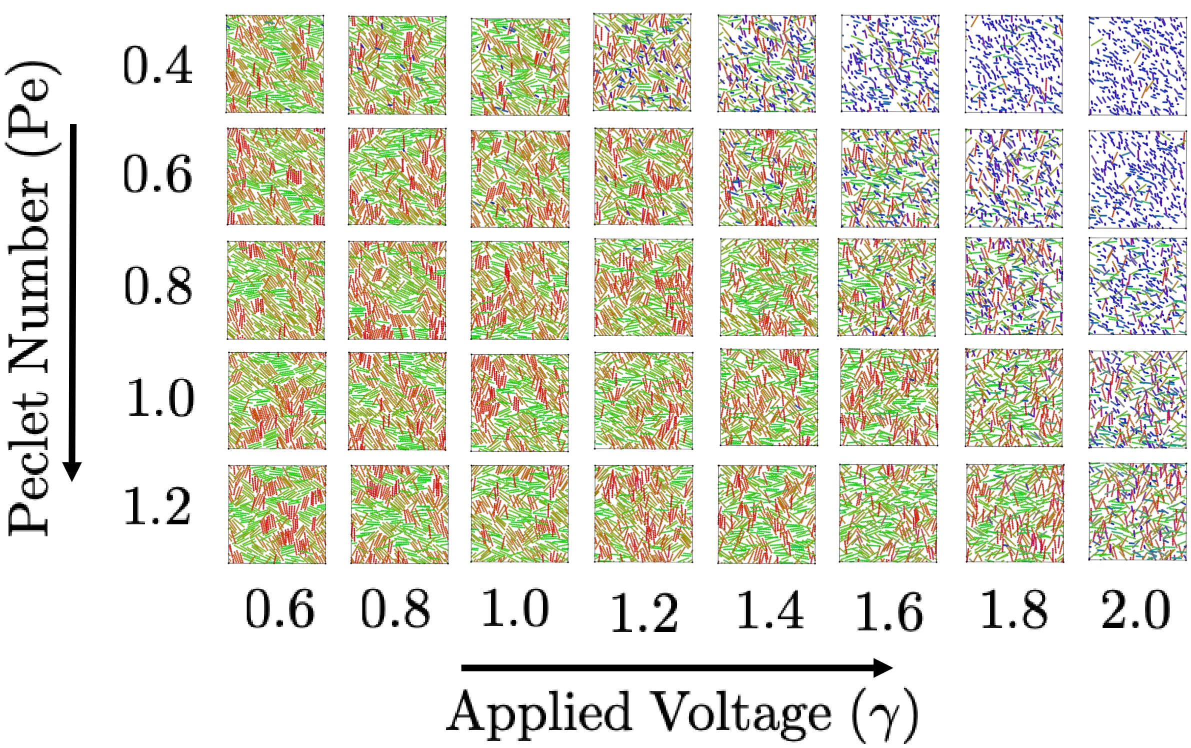

Figure S7: **Monte Carlo (MC) simulations at high surface coverage.** A mosaic of typical MC configurations after 10^5 MC steps per rod, viewed along the positive z axis. Rods are colored by orientation: red, green, and blue indicate alignment along the x-, y-, and z-directions, respectively. The Péclet number and dipole strength γ are varied in a system of $N = 300$ rods with aspect ratio $L/\sigma = 8$ at a surface coverage of $N\sigma/l^2 = 0.8$. All simulations are initialized with rods in an upright configuration.

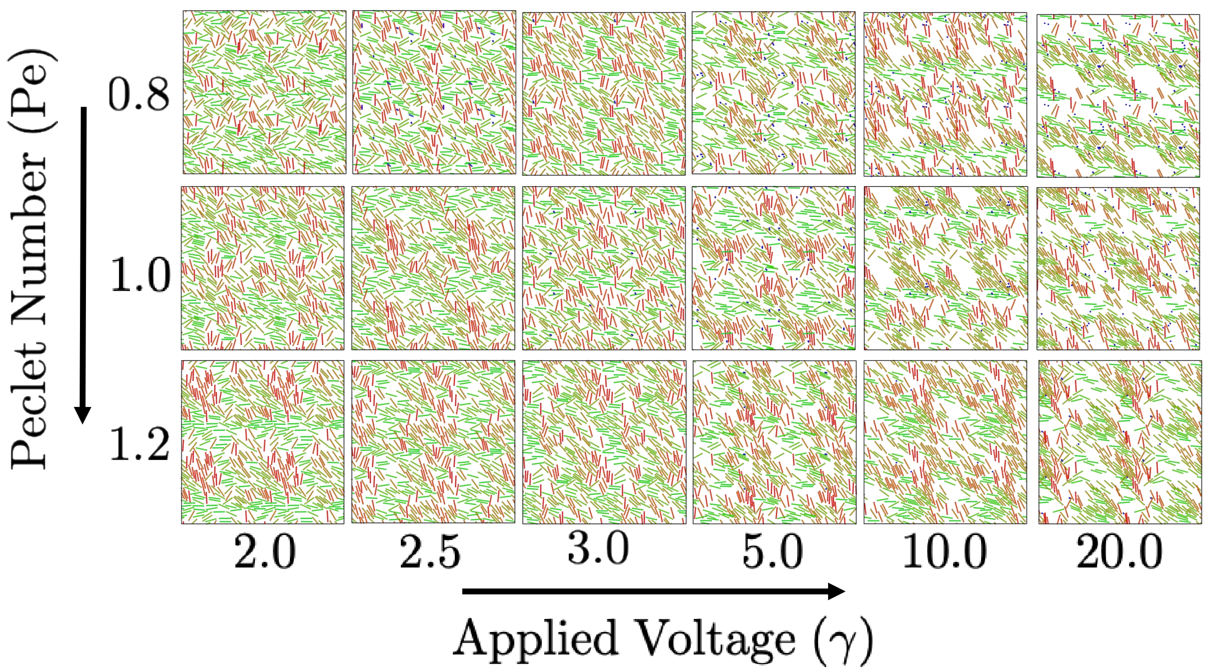

Figure S8: **Monte Carlo (MC) simulations at low surface coverage.** A mosaic of typical MC configurations after 10^5 MC steps per rod, viewed along the positive z axis. Rods are colored by their orientation: red, green, and blue indicate alignment along the x-, y-, and z-directions, respectively. The Péclet number and dipole strength γ are varied in a system of $N = 150$ rods with aspect ratio $L/\sigma = 8$ at a surface coverage of $N\sigma/l^2 = 0.4$. All simulations are initialized with rods lying flat. To better visualize clustering, each configuration is replicated once along both the x and y directions.

S1. Monte Carlo Simulation of Dipolar Rods under Confinement

The system under investigation involves a combination of steric and electrostatic interactions and consists of colloidal rods confined between two parallel conducting walls. Due to the dielectrophoretic effect, each colloid acquires a dipole moment aligned perpendicular to the electrodes, i.e. along the direction of the external electric field. To model this behavior, each rod is represented as a rigid linear chain of hard spheres of diameter σ, with each bead carrying a point dipole moment fixed along the z-axis. The dipole-dipole interaction between two point dipoles separated by a center-to-center distance r and with relative orientation θ is given by $U_{\text{dipole}} = \gamma\sigma^3(1 - 3\cos^2\theta)/(2r^3)$, where γ is the dimensionless dipolar strength (see main text). We use rods with an aspect ratio $L/\sigma = 8$, corresponding to the average length observed in the experimental system.

Each Monte Carlo step consists of a trial translation and rotation of a randomly selected rod. Rotations are performed using small random quaternions to enhance computational efficiency. The rods are confined between two conducting walls along the z-direction, with hard-wall boundary conditions, while periodic boundary conditions are applied in the x and y directions.

Dipolar interactions are anisotropic and long-ranged, requiring the use of Ewald summation. While Ewald summation is traditionally formulated for fully periodic three-dimensional systems, our system is confined in the z-direction. The lack of periodicity in the z-direction is resolved by noting that a perpendicular electric field between conducting electrodes induces an infinite series of image dipoles. We exploit this by explicitly constructing mirror images of all rods across the confining planes, effectively restoring periodicity along the z-direction and enabling the use of standard 3D Ewald summation. The real-space contribution is damped using the complementary error function, while the reciprocal-space sum is computed over a lattice of wavevectors. To improve efficiency, optimized bookkeeping is employed to incrementally update the reciprocal-space energy after each Monte Carlo move, significantly reducing computational cost.

Although the experimental system has a thickness of approximately 120σ, we use a simulation box of height 20σ, corresponding to an effective thickness of 40σ when accounting for the mirror image system. This reduction significantly enhances computational efficiency without compromising physical accuracy, as the dipoles are strongly attracted to the confining walls and exhibit negligible interaction with their distant images.

The computational cost remains high, accounting for mirror images and inter-rod interactions, each rod comprises 16 interacting dipolar beads, resulting in a total of 2400 dipoles for a system of $N = 150$ rods.

In experiments, rods are predominantly observed to lie flat against the confining wall. To reproduce this behavior, we introduce a gravitational potential that biases rods toward the bottom electrode. To avoid introducing multiple independent parameters such as diffusion coefficients, particle mass, or gravity strength, we characterize the influence of gravity using a single dimensionless Péclet number, $\mathrm{Pe} = v_s\sigma/D$, which quantifies the ratio of sedimentation velocity to diffusion. The gravitational potential is then expressed as $U_g = \mathrm{Pe}h$, where h is the height of a bead above the bottom wall.

Supplementary Fig. S7 presents MC simulation snapshots at a surface coverage of $N\sigma/l^2 = 0.8$, where l denotes the lateral box length. We explore a range of Péclet numbers, $0.4 \leq \mathrm{Pe} \leq 1.2$, and dipolar field strengths, $0.6 \leq \gamma \leq 2.0$. All simulations are initialized with rods in an upright configuration. We observe that higher Péclet numbers require stronger fields to maintain this orientation. Importantly, at this density, clustering of flat-lying rods is not observed, regardless of their effective weight or the applied field strength.

To better capture the behavior of the system, we subsequently reduced the surface coverage to $N\sigma/l^2 = 0.4$, consistent with typical experimental conditions, and extended the range of field strengths to $2 \leq \gamma \leq 20$. As shown in Supplementary Fig. S8, this setup reveals that increasing the field strength in a system initialized with flat-lying rods promotes dipolar clustering. This configuration enables a controlled investigation of clustering and alignment transitions.

S2. Analysis of porous structures

The pore area A_p recognition is performed with an image analysis where we detect all connected regions (voids, i.e. pores) in the binary image that meet specified size and shape criteria, which were set to isolate only relevant pore spaces. Any detected regions below a specific area threshold (e.g., noise or irrelevant gaps) were excluded from the analysis to ensure accurate pore size measurement. This threshold was chosen based on the known dimensions of the particles.

Moreover, the thickness of the network (L_N) is defined as the diameter of the largest sphere that fits inside the object and contains the point as $\tau(\vec{p}) = 2\max(\{r \mid \vec{p} \in \mathrm{sph}(\vec{x}, r) \subseteq \Omega, \vec{x} \in \Omega\})$

To achieve a smoother, more uniform surface, this method reduces irregularities by adjusting the thickness values of surface voxels. The main advantage of using this method is its ability to provide localized, consistent measurements of structural thickness, even in complex, irregular geometries.

S3. Percolation estimation

As noted in previous works, ϕ_p decreases when the polydispersity increases for a fixed average rod length. Specifically, in our system, the percolation threshold is governed by the weight-average rod length $\langle L \rangle_w$, which is greater than the mean length $\bar{L}$ due to the longer rods contributing more heavily to connectivity. This leads to a reduction in ϕ_p as the polydispersity increases. This relationship can be expressed as [1]

$$\phi_p = \frac{1}{2}\frac{D}{\langle L \rangle_w}\frac{1}{\frac{\Delta}{D} - 1},$$

where $\langle L \rangle_w = \frac{\int dL\, L^2 P(L)}{\int dL\, L P(L)}$, and Δ is the maximum separation between rods. For a Gaussian distribution, the weight-average length is $\langle L\rangle_w \approx \bar{L}+\frac{\sigma^2}{\bar{L}}$, which shows that even small variances lead to a decrease in the ϕ_p. In our system, with a mean rod length of L= 6.2 μm, and standard deviation of 2.43 μm, we estimate at least a 20% reduction in the ϕ_p due to polydispersity. Moreover, the presence of attractive interactions further reduces the ϕ_p and influences the network structure, as described by the expression:

$$\phi_p = \frac{1}{2}\frac{D}{L}\frac{1}{\frac{\Delta}{D}-1}\cdot\frac{1}{I_\parallel + I_\perp},$$

where $I_\parallel$ and $I_\perp$ account for the orientation-dependent contributions to connectivity. The polydispersity not only reduces ϕ_p but also alters the network topology, as longer rods act as structural backbones, while shorter rods fill gaps and improve packing.

For a monodisperse system of non-interacting rods, the percolation threshold can be approximated using the expression [2]:

$$\phi_c^{\mathrm{mono}} \approx \frac{4.5}{L/D}, \tag{1}$$

as for rods with L/D<10 $\phi_\mathrm{c} \approx (\mathrm{L/D})^{-1}$. The factor 4.5 was approximated from Monte Carlo simulation fittings of the data for two-dimensional overlapping and non-interacting rods, as reported in the literature [2, 3]. For rods with an aspect ratio of $L/D = 10$, this yields a threshold of $\phi_c^{\mathrm{mono}} \approx 45$ %. However, our system includes a significant polydispersity of $\pm$20%, which lowers the percolation threshold. This is because longer rods in a polydisperse distribution enhance connectivity by bridging gaps that shorter rods cannot span.

To account for the effect of polydispersity, we use a correction factor. Studies on systems with moderate polydispersity have shown that the percolation threshold decreases approximately by 20% compared to the monodisperse case. Thus, we apply a correction factor of 0.8 to adjust for the increased connectivity:

$$\phi_c \approx \phi_c^{\text{mono}} \times 0.8 = \frac{4.5}{10} \times 0.8 \approx 0.35 \tag{2}$$

This implies that the critical area fraction for our polydisperse system is approximately $\phi_c \approx 35\%$. At this percolation threshold, the rods can establish sufficient connectivity to form a spanning cluster in the 2D system, thereby achieving percolation.

S4. Supplementary Movies

MovieS1: Fluorescence movie of quasi-2D suspension of Brownian rods sedimented to the bottom electrode with the electric field off.

MovieS2: Movie of the network formation by turning on the AC field from a Brownian isotropic configuration to a network formation at 2 kHz and 6 V_{pp}.

MovieS3: Movies the quasi 2D-network at an equilibrium state at various field conditions, at 6 V_{pp} and 4, 6 and 8 kKz from left to right.

MovieS4: Movie of a single rod surrounded by tracer particles (polystyrene particles 700 nm diameter) to map the electrohydrodynamic flow fields around the rod at various field conditions.

MovieS5: Monte Carlo simulations movie of a 2D planar configuration of rods (color depicts orientations) at low field strength conditions.

MovieS6: Monte Carlo simulations movie of a 2D planar configuration of rods (color depicts orientations) at high field strength conditions hinting at the rod interaction and formation of a network.

References

[1] A.V. Kyrylyuk, and P. van der Schoot, Continuum percolation of carbon nanotubes in polymeric and colloidal media, Proc. Natl. Acad. Sci. U.S.A. 105 (24) 8221-8226, (2008).

[2] I. Balberg and N. Binenbaum, *Phys. Rev. B*, **28**, 3799–3812 (1983)

[3] E. M. Sevick, P. A. Monson and J. M. Ottino *Phys. Rev. A*, **38**, 5376–5383 (1988)